Clusterization and deformation of multi-Λ hypernuclei within a relativistic mean-field model

Yusuke Tanimura*
Department of Physics, Tohoku University, Sendai 980-8578, Japan
and Graduate Program on Physics for the Universe, Tohoku University, Sendai 980-8578, Japan

(Received 19 December 2018; published 21 March 2019)

Deformed multi-Λ hypernuclei are studied within a relativistic mean-field model. In this paper, I take some $N = Z$ "hyper-isotope" chains, i.e., ${}^{8+n}_{n\Lambda}$Be, ${}^{20+n}_{n\Lambda}$Ne, and ${}^{28+n}_{n\Lambda}$Si systems where $n = 2$, 4 for Be and $n = 2$, 8 for Ne and Si. A sign of two-${}^{6}_{2\Lambda}$He cluster structure is observed in the two-body correlation in ${}^{12}_{4\Lambda}$Be. In the Ne hyper-isotopes, the deformation is slightly reduced by addition of Λ hyperons, whereas it is significantly reduced or even disappears in the Si hyper-isotopes.

DOI: 10.1103/PhysRevC.99.034324

I. INTRODUCTION

Hypernuclear physics studies have been made both theoretically and experimentally [1,2]. A primary motivation is the unified understanding of the baryon-baryon interaction based on the flavor SU(3) symmetry. The knowledge of general baryon-baryon interactions is essential for the understanding of neutron-star matter, in which the hyperons would emerge at high densities. Hyperons could be a nondestructive probe of nuclear structure with strong interaction, since they are free from the Pauli principle of nucleons.

In any physics, precise information on hyperon-nucleon and hyperon-hyperon interactions is essential. However, it is difficult to perform nucleon-hyperon or hyperon-hyperon scattering experiments because of the short lifetimes of hyperons. The main strategy is to produce hyperon(s) in an ordinary nucleus via (K^-, π^-), (π^+, K^+), $(e, e'K^+)$, or (K^-, K^+) reactions to extract information on the interactions [1–4]. Most of the experimental data are limited to single-Λ hypernuclei, and there are also a few data for double-Λ and Ξ nuclei [3–10]. Double-Λ hypernuclei are of special importance since they provide information about hyperon-hyperon interaction.

Besides the original motivations for study of hypernuclear physics, the properties of nuclear systems with one or more hyperons have been found to be interesting. In particular, so-called "impurity effects" of Λ hyperon when a few of them are added to an ordinary nucleus have been of great interest. The impurity effects have been extensively studied with various theoretical models. The attractive N-Λ and Λ-Λ interactions and the absence of the Pauli principle lead to a variety of impurity effects in single- and double-Λ nuclei, such as shrinkage of intercluster distance [12–17], modification of deformation [18–26], extension of the drip line [27], emergence of new collective modes [28], change of fission barrier [30,31], and existence of "supersymmetric" or "genuine hypernuclear" states [12,32].

The multi-Λ system with more than two Λ particles also is intriguing. I emphasize that hypernuclei with multiple strangeness are expected to be produced in future experiments [11] although it is not feasible at the moment to produce them experimentally. In such systems, the Λ hyperon is no longer a small amount of "impurity" but would be regarded as a third constituent of the nuclear many-body system, giving another dimension to the nuclear chart. The properties of the hyperon different from the nucleon would bring about nontrivial structures of nuclear system. As a matter of fact, multistrangeness nuclei have been discussed in some theoretical calculations [14,33–44]. Those include the following: ${}^{6}_{2\Lambda}$He clusters in hypernuclei [14,33,34], hyperon halo [35–37,39], competition between Λ and Ξ hyperons in finite nuclei [38,43], shell structure [38], dense hypernuclei [38], binding energy systematics [42], Λ-Λ pairing correlation [44], and stability of light multistrange nuclei [40,41]. So far, to the best of my knowledge, the calculations have been limited to spherical systems except for the ones in Refs. [33,34,41], where a microscopic cluster model, a molecular orbital model, and a cluster model were applied to the Be hyper-isotopes, respectively. In Ref. [34], it was demonstrated that the Λ hyperons in ${}^{12}_{4\Lambda}$Be favor a localization around the two α clusters.

In this paper, I focus on the clusterization and deformation properties of multi-Λ systems. A relativistic mean-field (RMF) model is employed, without any assumption on spatial symmetry and cluster structure. The RMF is one of the widely used models for hypernuclei (see Ref. [45] for a review). I take the following $N = Z$ hyper-isotope chains: ${}^{8+n}_{n\Lambda}$Be, ${}^{20+n}_{n\Lambda}$Ne, and ${}^{28+n}_{n\Lambda}$Si systems, where $n = 2$, 4 for Be and $n = 2$, 8 for Ne and Si. In particular, an analysis on the cluster structure is made using the two-body correlation as well as the one-body density distribution.

The paper is organized as follows. In Sec. II, I introduce the RMF model employed in this work. In Sec. III, I present the results of the Be hyper-isotopes and discuss their structures with special attention to the cluster structure. In Sec. IV, I discuss the deformations of the Ne

*tanimura@nucl.phys.tohoku.ac.jp

and Si hyper-isotopes. In Sec. V, I give the summary and perspectives.

II. MODEL AND NUMERICAL DETAILS

To describe the multi-Λ hypernucleus, I use a meson-exchange model with nonlinear couplings for RMF theory [46]. The Lagrangian density is given by

$$\begin{aligned}\mathcal{L} &= \bar{\psi}_N(i\partial\!\!\!/ - m_N)\psi_N + \bar{\psi}_\Lambda(i\partial\!\!\!/ - m_\Lambda)\psi_\Lambda \\ &+ \frac{1}{2}(\partial_\mu\sigma)(\partial^\mu\sigma) - \frac{1}{2}m_\sigma^2\sigma^2 - \frac{c_3}{3}\sigma^3 - \frac{c_4}{4}\sigma^4 \\ &- \frac{1}{4}G^{\mu\nu}G_{\mu\nu} + \frac{1}{2}m_\omega^2\omega^\mu\omega_\mu + \frac{d_4}{4}(\omega^\mu\omega_\mu)^2 \\ &- \frac{1}{4}\vec{R}^{\mu\nu}\cdot\vec{R}_{\mu\nu} + \frac{1}{2}m_\rho^2\vec{\rho}^\mu\cdot\vec{\rho}_\mu - \frac{1}{4}F^{\mu\nu}F_{\mu\nu} \\ &- \bar{\psi}_N\left(g_{\sigma N}\sigma + g_{\omega N}\omega\!\!\!/ + g_{\rho N}\vec{\rho}\!\!\!/\cdot\vec{\tau} + eA\!\!\!/\frac{1-\tau_3}{2}\right)\psi_N \\ &- \bar{\psi}_\Lambda\left(g_{\sigma\Lambda}\sigma + g_{\omega\Lambda}\omega\!\!\!/ + \frac{f_{\omega\Lambda}}{4m_\Lambda}G_{\mu\nu}\sigma^{\mu\nu}\right)\psi_\Lambda, \end{aligned} \tag{1}$$

where ψ_N and ψ_Λ are nucleon and Λ hyperon fields, and $G^{\mu\nu} = \partial^\mu\omega^\nu - \partial^\nu\omega^\mu$, $\vec{R}^{\mu\nu} = \partial^\mu\vec{\rho}^\nu - \partial^\nu\vec{\rho}^\mu$, and $F^{\mu\nu} = \partial^\mu A^\nu - \partial^\nu A^\mu$ are the field tensors of the vector mesons ω and ρ and the photon, respectively. $\vec{\tau}$ is the Pauli matrix in the isospin space. In the present model, the ω-Λ tensor coupling is explicitly included in the model although the ω-N tensor coupling has not been considered in most of the existing RMF parametrizations. The main role of the tensor coupling is to modify the spin-orbit potential and the spin-orbit splittings of the single-particle energies. A quark model in Ref. [47] implies that the ω-Λ tensor coupling is stronger than the ω-N tensor coupling. The ω-Λ tensor coupling is known to be important to reproduce the small spin-orbit splittings observed in the single-particle spectra of Λ hyperon [48–50]. I take the PK1 parameter set [51] for the nucleon-meson couplings and a parameter set in Ref. [48] for Λ-meson couplings. In Ref. [48], $g_{\sigma\Lambda}$ is fitted to the binding energy of ${}^{40}_{\Lambda}$Ca ($g_{\sigma\Lambda} = 0.618 g_{\sigma N}$). The naive quark model value $g_{\omega\Lambda} = (2/3)g_{\omega N}$ is taken for the Yukawa coupling between Λ and ω. As for the tensor ω-Λ coupling, $f_{\omega\Lambda} = -g_{\omega\Lambda}$ from the quark model [47] is used as in Refs. [48,49]. The Λ hyperon mass m_Λ is taken to be 1115.6 MeV. This model with the parameters thus determined reproduces the observed binding energies of light to heavy single-Λ hypernuclei reasonably well [48,49]. In the present study, the pairing correlations among nucleons and Λ hyperons are not taken into account.

Here I make a remark on the Λ-Λ interaction. In principle, one should consider the mesons coupled solely to the hyperon as well as σ and ω mesons. There has been a discussion that the σ-ω RMF model underestimates the observed double-Λ binding energy $B_{\Lambda\Lambda}$ and Λ-Λ interaction energy $\Delta B_{\Lambda\Lambda}$ [38,52]. $B_{\Lambda\Lambda}$ and $\Delta B_{\Lambda\Lambda}$ are defined as follows,

$$B_{\Lambda\Lambda}\left({}^{A}_{2\Lambda}Z\right) = B\left({}^{A-2}Z\right) - B\left({}^{A}_{2\Lambda}Z\right), \tag{2}$$

$$\Delta B_{\Lambda\Lambda}\left({}^{A}_{2\Lambda}Z\right) = B_{\Lambda\Lambda}\left({}^{A}_{2\Lambda}Z\right) - 2B_{\Lambda}\left({}^{A-1}_{\Lambda}Z\right), \tag{3}$$

where $B({}^{A}Z)$ is the binding energy of a nucleus ${}^{A}Z$, and $B_\Lambda({}^{A-1}_{\Lambda}Z) = B({}^{A-1}_{\Lambda}Z) - B({}^{A-2}Z)$. In Refs. [38,52], the discrepancies between the experimental data and the RMF results were attributed to the contributions from strange σ^* and ϕ mesons which are coupled only to Λ hyperon. However, the discussion was based on the old data [3,5,6] for $B_{\Lambda\Lambda}$ and $\Delta B_{\Lambda\Lambda}$, whereas the $B_{\Lambda\Lambda}$ and $\Delta B_{\Lambda\Lambda}$ values in newer data are considerably smaller [4]. Table I lists the values of $B_{\Lambda\Lambda}$ and $\Delta B_{\Lambda\Lambda}$ obtained with the present RMF model in comparison with the experimental values (see also Table I in Ref. [52]). It appears that the present RMF results without σ^* and ϕ mesons agree better with the newer data. Nevertheless, it has to be noted that the effect of beyond-mean-field correlations which could be significant in the light systems is missing in RMF, although there would be a partial cancellation of the correlation energies upon the subtraction in Eq. (2). Moreover, the experimental $B_{\Lambda\Lambda}$ and $\Delta B_{\Lambda\Lambda}$ values were deduced under some assumption on the formation and decay processes of the double-Λ nuclei [4]. Therefore, I leave discussions on extra Λ-Λ interaction and correlation for future works and adopt the phenomenological model in Eq. (1) fitted only to a single-Λ nucleus. More of new data, especially of heavier systems, from the ongoing analyses of the J-PARC E-07 experiment are awaited [9,10].

The model Lagrangian given above is solved within the mean-field and the no-sea approximations. I assume time-reversal invariance and charge conservation of the mean-field state, i.e., the time-odd or charged vector fields vanish. The only nonzero components are their timelike and neutral

TABLE I. The double-Λ binding energies $B_{\Lambda\Lambda}$ and Λ-Λ interaction energies $\Delta B_{\Lambda\Lambda}$ obtained with the present RMF model. For comparison, the experimental data in Refs. [3,4,9] are also listed. Note that the values of $B_{\Lambda\Lambda}$ and $\Delta B_{\Lambda\Lambda}$ for ${}^{6}_{2\Lambda}$He from Ref. [4] are given by the weighted average of NAGARA event ($B_{\Lambda\Lambda} = 6.91 \pm 0.16$ MeV and $\Delta B_{\Lambda\Lambda} = 0.67 \pm 0.17$ MeV) [7] and MIKAGE event ($B_{\Lambda\Lambda} = 10.06 \pm 1.72$ MeV and $\Delta B_{\Lambda\Lambda} = 3.82 \pm 1.72$ MeV) [8]. The former have been uniquely identified as ${}^{6}_{2\Lambda}$He [4,7] whereas the latter was only found most probable to be ${}^{6}_{2\Lambda}$He [4,8]. The data of Ref. [9] are the very recent results of the MINO event in the J-PARC E-07 experiment, the candidates of which are ${}^{10}_{2\Lambda}$Be, ${}^{11}_{2\Lambda}$Be (most likely), and ${}^{12}_{2\Lambda}$Be.

	$B_{\Lambda\Lambda}$ (MeV)				$\Delta B_{\Lambda\Lambda}$ (MeV)			
	RMF	Exp. [9]	Exp. [4]	Exp. [3]	RMF	Exp. [9]	Exp. [4]	Exp. [3]
${}^{6}_{2\Lambda}$He	4.24		6.93 ± 0.16	10.9 ± 0.6	1.08		0.70 ± 0.17	4.7 ± 0.6
${}^{10}_{2\Lambda}$Be	13.23	(15.05 ± 0.11)	11.90 ± 0.13	17.7 ± 0.4	0.59	(1.63 ± 0.14)	-1.52 ± 0.15	4.3 ± 0.4
${}^{13}_{2\Lambda}$B			23.3 ± 0.7	27.5 ± 0.7			0.6 ± 0.8	4.8 ± 0.7

components, ω^0, ρ_3^0, and A^0, where the subscript 3 on the ρ meson field means the third component in the isospace.

The scalar-isoscalar density ρ_S and vector-isoscalar and vector-isovector densities j^0 and j_3^0 of nucleons are defined in terms of the single-particle wave functions of nucleon $\psi_k^{(N)}$ as

$$\rho_S(\boldsymbol{r}) = \sum_{k\in\mathrm{occ}} \bar{\psi}_k^{(N)}(\boldsymbol{r})\psi_k^{(N)}(\boldsymbol{r}), \tag{4}$$

$$j^0(\boldsymbol{r}) = \sum_{k\in\mathrm{occ}} \bar{\psi}_k^{(N)}(\boldsymbol{r})\gamma^0\psi_k^{(N)}(\boldsymbol{r}), \tag{5}$$

$$j_3^0(\boldsymbol{r}) = \sum_{k\in\mathrm{occ}} \bar{\psi}_k^{(N)}(\boldsymbol{r})\gamma^0\tau_3\psi_k^{(N)}(\boldsymbol{r}), \tag{6}$$

where k runs over the occupied nucleon states. The scalar, vector, and tensor densities of Λ hyperon are defined in terms of the single-particle wave function of Λ hyperon $\psi_k^{(\Lambda)}$ as

$$\rho_{S\Lambda}(\boldsymbol{r}) = \sum_{k\in\mathrm{occ}} \bar{\psi}_k^{(\Lambda)}(\boldsymbol{r})\psi_k^{(\Lambda)}(\boldsymbol{r}), \tag{7}$$

$$j_\Lambda^0(\boldsymbol{r}) = \sum_{k\in\mathrm{occ}} \bar{\psi}_k^{(\Lambda)}(\boldsymbol{r})\gamma^0\psi_k^{(\Lambda)}(\boldsymbol{r}), \tag{8}$$

$$\boldsymbol{V}_{T\Lambda}(\boldsymbol{r}) = \sum_{k\in\mathrm{occ}} \bar{\psi}_k^{(\Lambda)}(\boldsymbol{r})i\boldsymbol{\alpha}\psi_k^{(\Lambda)}(\boldsymbol{r}), \tag{9}$$

where k here runs over the occupied Λ-hyperon states.

The equations of motion for the meson and electromagnetic fields read

$$\left(-\nabla^2 + m_\sigma^2\right)\sigma = -g_{\sigma N}\rho_S - c_3\sigma^2 - c_4\sigma^3 - g_{\sigma\Lambda}\rho_{S\Lambda}, \tag{10}$$

$$\left(-\nabla^2 + m_\omega^2\right)\omega^0 = g_{\omega N}j^0 - d_4(\omega^0)^3 + g_{\omega\Lambda}j_\Lambda^0 + \frac{f_{\omega\Lambda}}{2m_\Lambda}\nabla\cdot\boldsymbol{V}_{T\Lambda}, \tag{11}$$

$$\left(-\nabla^2 + m_\rho^2\right)\rho_3^0 = g_{\rho N}j_3^0, \tag{12}$$

$$-\nabla^2 A^0 = \frac{e}{2}\left(j^0 - j_3^0\right). \tag{13}$$

Notice that there are the contributions from the Λ hyperon to the sources of the σ and ω fields. The ρ and A fields will also be affected by Λ hyperon through the modification on the nucleon densities in the self-consistent calculation for hypernuclei.

The Dirac equation for the nucleon single-particle wave function is given by

$$[-i\boldsymbol{\alpha}\cdot\nabla + V_N + \beta(m_N + S_N)]\psi_k^{(N)} = \epsilon_k\psi_k^{(N)}, \tag{14}$$

where

$$S_N = g_{\sigma N}\sigma, \tag{15}$$

$$V_N = g_{\omega N}\omega^0 + g_{\rho N}\rho_3^0\tau_3 + eA^0\frac{1-\tau_3}{2}. \tag{16}$$

Note that $\tau_3 = +1$ for neutron and $\tau_3 = -1$ for proton. The Dirac equation for the single-particle wave function of Λ hyperon is given by

$$[-i\boldsymbol{\alpha}\cdot\nabla + V_\Lambda + \beta(m_\Lambda + S_\Lambda) + T_\Lambda]\psi_k^{(\Lambda)} = \epsilon_k\psi_k^{(\Lambda)}, \tag{17}$$

where

$$S_\Lambda = g_{\sigma\Lambda}\sigma, \tag{18}$$

$$V_\Lambda = g_{\omega\Lambda}\omega^0, \tag{19}$$

$$T_\Lambda = \frac{f_{\omega\Lambda}}{2m_\Lambda}i\beta\boldsymbol{\alpha}\cdot(-\nabla\omega^0). \tag{20}$$

The set of nonlinear equations, Eqs. (4)–(20), are solved self-consistently. In the numerical calculations, the single-particle wave functions are represented on a three-dimensional lattice in the real space [53]. To avoid the fermion doubling, the derivative in the Dirac equation is computed in the momentum space with the fast Fourier transform [54], for which I use the FFTW library [55]. The damped gradient iteration technique [56,57] is used to solve the self-consistent mean-field equations (see also Ref. [58]). The Klein-Gordon equations for the mesons and the Poisson equation for the Coulomb field are solved in the momentum space with the fast Fourier transform. For solving the Poisson equation in the momentum space, I employ the same method as in Refs. [59,60]. Calculations are performed with 24^3 mesh points and lattice spacing of 0.8 fm.

III. RESULTS AND DISCUSSION: BE HYPER-ISOTOPES

First, I show the results of ^{8}Be, $^{10}_{2\Lambda}$Be, and $^{12}_{4\Lambda}$Be.

In the density plots in this paper, only the neutron and Λ densities will be shown because the neutron and proton densities are almost the same in the $N = Z$ hyper-isotopes. From here on, the neutron and Λ densities will be referred to as ρ_n and ρ_Λ, respectively,

$$\rho_n \equiv \tfrac{1}{2}\left(j^0 + j_3^0\right), \tag{21}$$

$$\rho_\Lambda \equiv j_\Lambda^0. \tag{22}$$

In Fig. 1, the density distributions of neutron and Λ hyperon are presented. The neutron densities ρ_n are drawn by contour map, while the Λ densities ρ_Λ are drawn by color (grayscale) map. Figure 1(a) shows the ground state of ^{8}Be, Figs. 1(b) and 1(c) show the ground state of $^{10}_{2\Lambda}$Be with the two Λ hyperons in the s orbital (denoted as $^{10}_{2\Lambda s}$Be) and $^{10}_{2\Lambda}$Be with the two Λ hyperons in the p orbital (denoted as $^{10}_{2\Lambda p}$Be), respectively, and Fig. 1(d) shows the ground state of $^{12}_{4\Lambda}$Be. $^{10}_{2\Lambda p}$Be is obtained by having the Λ's occupy the second lowest single-particle level during the self-consistent iterations. In Fig. 2, I show the central mean-field potentials of neutron and Λ,

$$U_n \equiv V_n + S_n, \tag{23}$$

$$U_\Lambda \equiv V_\Lambda + S_\Lambda. \tag{24}$$

In Fig. 2, the dotted line represents ^{8}Be, dot-dashed and double-dot-dashed lines represent $^{10}_{2\Lambda s}$Be and $^{10}_{2\Lambda p}$Be, respectively, and the solid line represents $^{12}_{4\Lambda}$Be.

A. Structures of $^{10}_{2\Lambda}$Be with Λ's in s or p orbitals

Here I compare the structures of ^{8}Be, $^{10}_{2\Lambda s}$Be, and $^{10}_{2\Lambda p}$Be. Note that the two Λ hyperons in $^{10}_{2\Lambda p}$Be occupy the p state along the symmetry axis of the system [Fig. 1(c)]. Such a

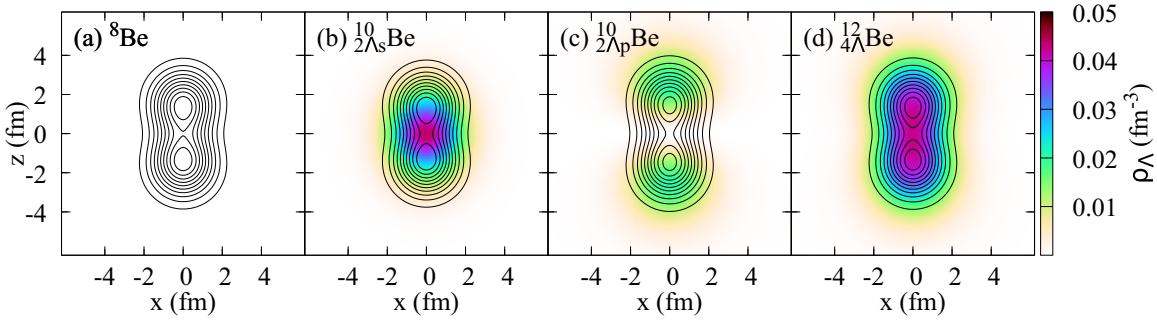

FIG. 1. Neutron and Λ hyperon density distributions of (a) ^{8}Be, (b) $^{10}_{2\Lambda}$Be with Λ's in s orbital ($^{10}_{2\Lambda_s}$Be), (c) $^{10}_{2\Lambda}$Be with Λ's in p orbital($^{10}_{2\Lambda_p}$Be), and (d) $^{12}_{4\Lambda}$Be. The neutron densities ρ_n are shown by contour map, which starts from 0.1 fm^{-3} with the increments by 0.1 fm^{-3}. The Λ-hyperon densities ρ_Λ are shown by color (grayscale) map. The densities at $y = 0$ as a function of z and x are plotted. z (vertical) is the symmetry axis.

configuration does not have an analog state in the nonstrange isotopes, e.g., ^{10}Be where two neutrons are added to ^{8}Be instead of Λ hyperons [1,12,21,29,32]. Thus, this state is unique in the hypernucleus and is called a "supersymmetric" or "genuine hypernuclear" state [12,32].

One sees in Figs. 1(a)–1(d) that the nucleon distributions in the Be hyper-isotopes exhibit a well-developed α cluster structure. In $^{10}_{2\Lambda_s}$Be, the Λ particles stay around the middle between the two α's [Fig. 1(b)]. Accordingly, the central potential for neutron, as seen from the dot-dashed curve in Fig. 2(a), becomes deeper at the middle, due to the additional attraction by the Λ hyperons. The nucleons are attracted toward the middle of the system, which leads to a slight reduction of the distance between the two α clusters. On the other hand, in $^{10}_{2\Lambda_p}$Be in which the two Λ hyperons are in the p orbital, the potential becomes shallower and wider [double-dot-dashed curve Fig. 2(a)], and the nucleon distribution is stretched along the z axis, which is the axis of symmetry. These effects are seen in the quadrupole deformation parameter β_2, the root-mean-squared (rms) radius R of the system, and the α-α distance $D_{\alpha\alpha}$, which are summarized in Table II. The quadrupole deformation parameter and the rms radius are defined as

$$\beta_2 = \frac{4\pi}{5}\frac{\int d^3r\, r^2 Y_{20}\rho}{\int d^3r\, r^2\rho} \tag{25}$$

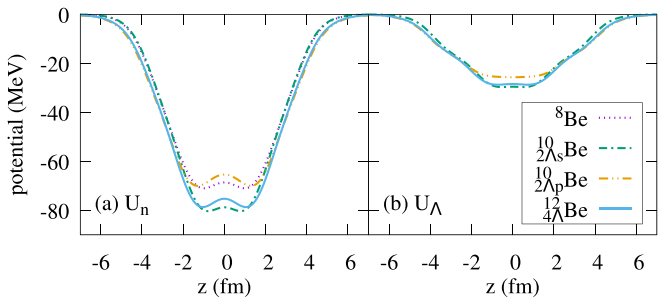

FIG. 2. Central potentials of (a) neutron and (b) Λ hyperon of Be hyper-isotopes, ^{8}Be, $^{10}_{2\Lambda_s}$Be, $^{10}_{2\Lambda_p}$Be, and $^{12}_{4\Lambda}$Be along the symmetry axis. In $^{10}_{2\Lambda_s}$Be and $^{10}_{2\Lambda_p}$Be, the two Λ hyperons occupy the s and the p orbital, respectively.

and

$$R = \sqrt{\frac{\int d^3r\, r^2\rho}{\int d^3r\, \rho}}, \tag{26}$$

respectively, where ρ is the density of the particle that is considered. The α-α distance $D_{\alpha\alpha}$ is defined as the distance between the two maxima of the nucleon density distribution along z axis. One observes that $\beta_{2N}(^{10}_{2\Lambda_s}\text{Be}) < \beta_{2N}(^{8}\text{Be}) < \beta_{2N}(^{10}_{2\Lambda_p}\text{Be})$, and the same relations hold for R_N and $D_{\alpha\alpha}$ as well. Note that a similar result was obtained also in Ref. [21] with an antisymmetrized molecular dynamics model for $^{9}_{\Lambda}$Be when a Λ particle occupies either s or p orbital.

B. Clusterization in $^{12}_{4\Lambda}$Be

In $^{12}_{4\Lambda}$Be with two more Λ's, the density of Λ hyperon becomes strongly deformed [Fig. 1(d)], and the nucleon density recovers nearly the same deformation, radius, and α-α distance as in the ^{8}Be normal isotope (see Table II). However, as seen in Fig. 3, the Λ hyperon density distribution does not have a neck at the middle as the nucleon density distribution does. An interpretation to this behavior of the Λ hyperon density is that the Λ's are not as tightly bound to α as the nucleons are, so they can move more freely between the two clusters. As a consequence, the density distribution at the mean-field level becomes flat at the middle.

TABLE II. Quadrupole deformation parameters β_2, root-mean-squared radii R, and the distance between the two α's $D_{\alpha\alpha}$ of the Be hyper-isotope chain. β_{2N} and R_N are deformation parameter and radius calculated from the nucleon density, and $\beta_{2\Lambda}$ and R_Λ are calculated from the Λ hyperon density. N_Λ is the number of Λ hyperons. Λ_s and Λ_p for $N_\Lambda = 2$ mean that the Λ particles are in s and p orbitals, respectively.

N_Λ	β_{2N}	$\beta_{2\Lambda}$	R_N (fm)	R_Λ (fm)	$D_{\alpha\alpha}$ (fm)
			Be hyper-isotopes		
0	0.67		2.43		2.8
$2\Lambda_s$	0.64	0.18	2.36	2.59	2.6
$2\Lambda_p$	0.72	0.71	2.49	4.27	3.0
4	0.68	0.57	2.42	3.49	2.8

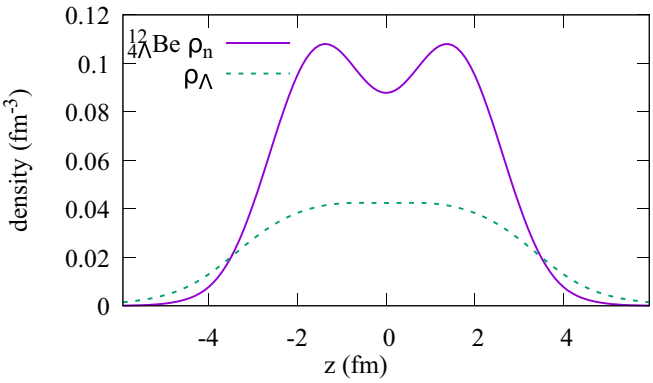

FIG. 3. Comparison between the neutron (solid curve) and Λ hyperon (dashed curve) densities in $^{12}_{4\Lambda}$Be along the symmetry axis.

I make a further analysis on the cluster structure in $^{12}_{4\Lambda}$Be, using the fermion localization function [61–66]. The localization function is a measure of localization, which is related to the spatial two-body correlation between two like-spin fermions of the same kind. The localization function for a particle of kind $q = n$, p, or Λ with spin $\sigma = +1/2$ (↑) or $-1/2$ (↓) is defined as

$$\mathcal{C}_{q\sigma}(\boldsymbol{r}) = \left[1 + \left(\frac{\rho_{q\sigma}\tau_{q\sigma} - \boldsymbol{j}_{q\sigma}^2 - \frac{1}{4}(\nabla\rho_{q\sigma})^2}{\rho_{q\sigma}\tau_{q\sigma}^{\rm TF}}\right)^2\right]^{-1}. \quad (27)$$

Here, $\tau_{q\sigma}^{\rm TF} = \frac{3}{5}(6\pi^2)^{2/3}\rho_{q\sigma}^{5/3}$ is the Thomas-Fermi kinetic energy density, and

$$\tau_{q\sigma}(\boldsymbol{r}) = \frac{1}{2}\sum_{k\in q,{\rm occ}}[\nabla\psi_k^\dagger(\boldsymbol{r})]\cdot(1+2\sigma\Sigma^3)[\nabla\psi_k(\boldsymbol{r})] \quad (28)$$

and

$$\boldsymbol{j}_{q\sigma}(\boldsymbol{r}) = {\rm Im}\left[\sum_{k\in q,{\rm occ}}\psi_k^\dagger(\boldsymbol{r})(1+2\sigma\Sigma^3)\nabla\psi_k(\boldsymbol{r})\right], \quad (29)$$

where $\Sigma^3 = \begin{pmatrix}\sigma_z & 0\\ 0 & \sigma_z\end{pmatrix}$ is the spin operator and k runs over the occupied states of the fermion kind q. Note that $\boldsymbol{j}_{q\sigma} = \boldsymbol{0}$, $\rho_{q\uparrow} = \rho_{q\downarrow}$, and $\tau_{q\uparrow} = \tau_{q\downarrow}$ in the present case with the time-reversal symmetry.

A value of $\mathcal{C}_{q\sigma}$ close to one is the sign of localization [62], which means that the probability of finding two particles with the same spin close to each other is very low. $\mathcal{C}_{q\sigma} \approx 1$ simultaneously for all the spin-isospin combinations is a minimal necessary condition of α clusterization [62]. The α-cluster correlation in terms of the localization function can be naturally extended to $^{6}_{2\Lambda}$He: $\mathcal{C}_{q\sigma} \approx 1$ at the same spacial region for $n\uparrow$, $n\downarrow$, $p\uparrow$, $p\downarrow$, $\Lambda\uparrow$, and $\Lambda\downarrow$ implies $^{6}_{2\Lambda}$He clusterization. In the present case with $N = Z$ and time-reversal symmetry, the wave functions of neutron and proton are approximately the same, and the spin-up and spin-down components are exactly the same, so it suffices to consider only the neutron spin-up and Λ spin-up components.

Since the localization is not a meaningful quantity in the regions where the one-body density is close to zero, we look at the localization function multiplied by the normalized one-body density

$$\overline{\mathcal{C}}_{q\sigma}(\boldsymbol{r}) = \mathcal{C}_{q\sigma}(\boldsymbol{r})\frac{\rho_{q\sigma}(\boldsymbol{r})}{\max\rho_{q\sigma}(\boldsymbol{r})}, \quad (30)$$

as was done in Ref. [63].

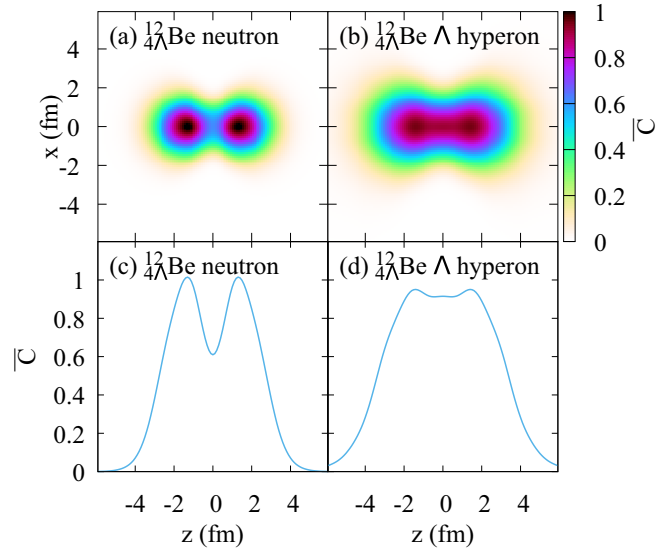

FIG. 4. Localization functions $\overline{\mathcal{C}}_{q\sigma} = \mathcal{C}_{q\sigma}\frac{\rho_{q\sigma}}{\max\rho_{q\sigma}}$ on zx plane in $^{12}_{4\Lambda}$Be for (a) $(q\sigma) =$ (neutron ↑) and (b) $(q\sigma) = (\Lambda\uparrow)$. In panels (c) and (d) are plotted $\overline{\mathcal{C}}_{n\uparrow}$ and $\overline{\mathcal{C}}_{\Lambda\uparrow}$, respectively, along the symmetry axis.

In Fig. 4, the neutron and Λ-hyperon localization measures, $\overline{\mathcal{C}}_{n\uparrow}$ and $\overline{\mathcal{C}}_{\Lambda\uparrow}$ defined by Eq. (30) are plotted. The neutron localization has two strong peaks at the positions of the two α clusters, indicating the α-cluster correlation. More interestingly, the localization of Λ hyperon in Figs. 4(b) and 4(d) takes the values slightly more around the α clusters than at the region in between, which was not seen in the one-body density distribution in Fig. 3. This implies the existence of two $^{6}_{2\Lambda}$He clusters, although the localization of the Λ hyperons is much more obscure than the nucleon.

I remark also that the rms radius of Λ hyperon in $^{12}_{4\Lambda}$Be is significantly larger than that of nucleon ($R_\Lambda/R_N = 3.49/2.42 \approx 1.4$) although the number of Λ particles in $^{12}_{4\Lambda}$Be is the same as those of neutrons and protons. This is because the Λ particles are more weakly bound in a shallow potential (≈ -30 MeV) as one sees in Fig. 2(b). In particular, the last occupied orbital in $^{12}_{4\Lambda}$Be is bound only by 1.3 MeV, which makes a halo- or skinlike structure of Λ. Similar results have been obtained also in Refs. [35,36,39] for spherical multi-Λ systems.

IV. RESULTS AND DISCUSSION: NE AND SI HYPER-ISOTOPES

Next, I investigate Ne and Si hyper-isotopes with two and eight Λ particles: ^{20}Ne, $^{22}_{2\Lambda}$Ne, $^{28}_{8\Lambda}$Ne, ^{28}Si, $^{30}_{2\Lambda}$Si, and $^{36}_{8\Lambda}$Si.

In Fig. 5 are shown the density distributions of neutrons and Λ hyperons in ^{20}Ne, $^{22}_{2\Lambda}$Ne, and $^{28}_{8\Lambda}$Ne. In Figs. 5(a)–5(e),

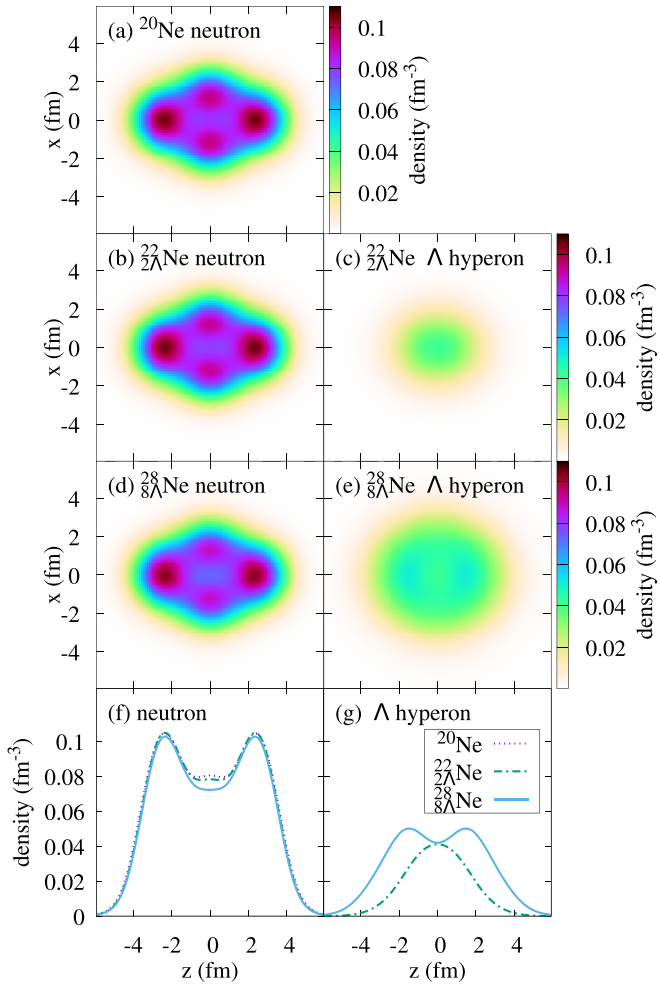

FIG. 5. The density distributions on zx plane in the Ne hyper-isotopes, (a) neutron in ^{20}Ne, (b) neutron in $^{22}_{2\Lambda}$Ne, (c) Λ hyperon in $^{22}_{2\Lambda}$Ne, (d) neutron in $^{28}_{8\Lambda}$Ne, and (e) Λ hyperon in $^{28}_{8\Lambda}$Ne. Panels (f) and (g) show the comparisons of neutron and Λ densities along the symmetry axis, respectively, among the hyper-isotopes. The z axis (horizontal) is the symmetry axis.

the density distributions of individual hyper-isotopes on the zx plane are plotted, and in Figs. 5(f) and 5(g), the densities of different hyper-isotopes along the symmetry axis are compared. Notice that the axis of symmetry is horizontal in Fig. 5. The quadrupole deformation parameters β_2 and radii R are tabulated in Table III.

The nucleon density distributions in the Ne hyper-isotopes has prolate deformation. The density distributions of Λ particles are also prolately deformed so that they gain binding energy from the attractive interaction with nucleons. From Table III, one sees that the nucleon quadrupole deformation β_{2N} decreases from ^{20}Ne to $^{22}_{2\Lambda}$Ne and from $^{22}_{2\Lambda}$Ne to $^{28}_{8\Lambda}$Ne. The deformation of Λ hyperon $\beta_{2\Lambda}$ also decreases from the 2Λ to the 8Λ isotopes.

One also observes in the density distributions that the hole at the center of neutron density becomes significantly depressed when there are eight Λ hyperons. In Fig. 6 are shown the central mean fields of neutrons and Λ hyperons in the

TABLE III. Quadrupole deformation parameters β_2 and root-mean-squared radii R of the Ne and Si hyper-isotope chains. β_{2N} and R_N are deformation parameter and radius calculated from the nucleon density, and $\beta_{2\Lambda}$ and R_Λ are calculated from the Λ-hyperon density. N_Λ is the number of Λ hyperons.

N_Λ	β_{2N}	$\beta_{2\Lambda}$	R_N (fm)	R_Λ (fm)
		Ne hyper-isotopes		
0	0.43		2.82	
2	0.40	0.16	2.81	2.53
8	0.38	0.09	2.82	3.33
		Si hyper-isotopes		
0	−0.31		3.14	
2	−0.22	−0.12	2.95	2.49
8	0.00	0.00	2.92	3.14

Ne hyper-isotopes. As seen from the difference between the dotted and the dot-dashed curves in Fig. 6(a), in $^{22}_{2\Lambda}$Ne, the Λ particles in the lowest s-shell orbital give an extra contribution to the central potential that shifts down the bottom of it. When six more Λ particles are added ($^{28}_{8\Lambda}$Ne), they occupy the p-shell orbitals whose densities are very low around the origin [compare the solid and dot-dashed curves in Fig. 5(g)]. Consequently, the mean-field potential shown with the solid curve in Fig. 6(a) is deepened at regions where $z \approx \pm 2$ fm. A similar thing happens in the other directions as well. This change in the potential induces the deeper hole in the nucleon density of $^{28}_{8\Lambda}$Ne.

In the Si hyper-isotope chain, the shape variation is more drastic. In Fig. 7, the density distributions of neutron and Λ hyperon in ^{28}Si, $^{30}_{2\Lambda}$Si and $^{36}_{8\Lambda}$Si are shown, and the quadrupole deformations and radii are tabulated in Table III. ^{28}Si is oblately deformed. With two Λ hyperons, the oblate deformation is relaxed from $\beta_{2N} = -0.31$ to -0.22. With eight Λ hyperons, the spherical magicity of Λ overcomes the nucleon deformation, and the system becomes spherical. The nucleons are in $(1s_{1/2})^4(1p_{3/2})^8(1p_{1/2})^4(1d_{5/2})^{12}$ configuration in $^{36}_{8\Lambda}$Si. Similar results are obtained also in the previous works on single-Λ hypernuclei [18,22]. Since the potential energy surface of ^{28}Si is rather flat as a function of the quadrupole deformation, the Si hyper-isotopes with one, two, or eight Λ hyperons, which resist against deformation, easily go toward a spherical shape [18,22].

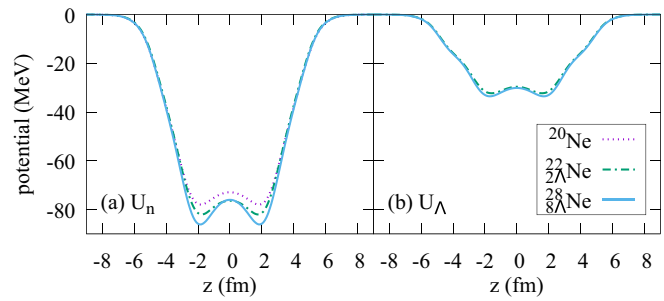

FIG. 6. Central potentials of (a) neutron and (b) Λ hyperon of Ne hyper-isotopes, ^{20}Ne, $^{22}_{2\Lambda}$Ne, and $^{28}_{8\Lambda}$Ne.

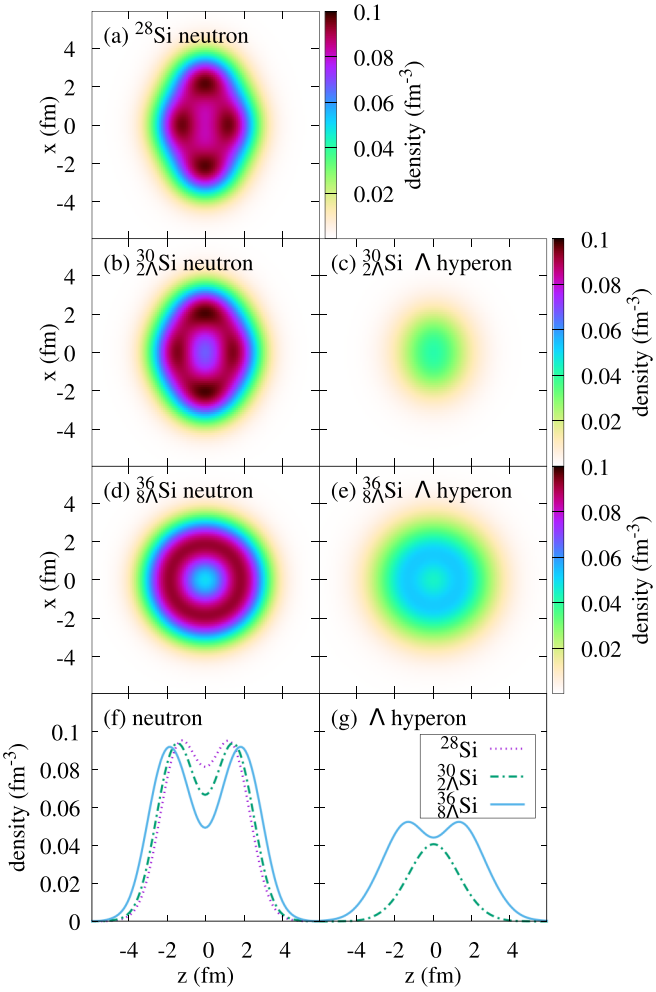

FIG. 7. Neutron and Λ hyperon density distributions of Si hyper-isotopes, ^{28}Si, $^{30}_{2\Lambda}$Si, and $^{36}_{8\Lambda}$Si. The z axis (horizontal) is the symmetry axis.

In view of the flat potential energy surface of ^{28}Si, the predicted deformations of the Si hyper-isotopes may be model dependent. To see the model dependence of the results of the Si hyper-isotopes, I have made the same calculations with different nucleon-meson effective interactions: NL3 [67], NLSH [68], and TM2 [69]. For each of the given nucleon-meson interaction, I refitted the Λ-σ coupling constant $g_{\sigma\Lambda}$ in the same way for $^{40}_{\Lambda}$Ca as in Ref. [48]. The resultant values are $g_{\sigma\Lambda} = 0.6186 g_{\sigma N}$ for NL3, $g_{\sigma\Lambda} = 0.6201 g_{\sigma N}$ for NLSH, and $g_{\sigma\Lambda} = 0.6236 g_{\sigma N}$ for TM2. The quadrupole deformations of nucleon density distribution of the Si hyper-isotopes obtained with the different interactions are summarized in Table IV. Although they give similar β_{2N} values for ^{28}Si except for TM2, the β_{2N} value for $^{30}_{2\Lambda}$Si becomes zero for all the interactions other than PK1. When $\beta_{2N} = 0$, $\beta_{2\Lambda} = 0$ in all cases shown in Table IV.

As in the case of the Be hyper-isotopes, the radii of Λ hyperon density distributions in Ne and Si are larger than that of nucleon when Λ's occupy the p-shell orbitals (see Table III).

TABLE IV. β_{2N} values in the ground states of the Si hyper-isotopes obtained with different effective interactions, NL3 [67], NLSH [68], and TM2 [69] as well as PK1.

	β_{2N}			
	PK1	NL3	NLSH	TM2
^{28}Si	−0.31	−0.30	−0.29	0.00
$^{30}_{2\Lambda}$Si	−0.22	0.00	0.00	0.00
$^{36}_{8\Lambda}$Si	0.00	0.00	0.00	0.00

V. SUMMARY AND PERSPECTIVES

In this work, I have investigated the clusterization and deformation properties of $N = Z$ multi-Λ nuclei, $^{8+n}_{n\Lambda}$Be, $^{20+n}_{n\Lambda}$Ne, and $^{28+n}_{n\Lambda}$Si, where $n = 2, 4$ for Be and $n = 2, 8$ for Ne and Si.

I employed a relativistic mean-field model with meson-exchange interaction. One of the three coupling constants of the Λ-meson couplings is fitted to the binding energy of a single-Λ hypernucleus $^{40}_{\Lambda}$Ca, and the remaining two are fixed by quark models.

In the $^{10}_{2\Lambda}$Be nucleus, when the two Λ's occupy the s (p) orbital, the intercluster distance decreases (increases), as in the case of $^{9}_{\Lambda}$Be [21].

In the $^{12}_{4\Lambda}$Be nucleus, a sign of two-$^{6}_{2\Lambda}$He cluster structure is observed in the two-body correlation embedded in the localization function, consistent with the result obtained in Ref. [34]. Notice that to draw a conclusion on the cluster correlation, one needs to perform a beyond-mean-field calculation which properly takes into account the quantum dynamics of shape degrees of freedom and to analyze the spatial and spin-isospin correlations in the many-body wave function.

When Λ hyperons fill up the spherical major shells (s and p shells in the present study) but nucleons favor deformation, there is a competition between them due to the attractive interaction between the nucleons and the Λ hyperons. In the Ne hyper-isotopes $^{22}_{2\Lambda}$Ne and $^{28}_{8\Lambda}$Ne, the nucleon density distributions are slightly less deformed than in the normal isotope ^{20}Ne, attracted by the Λ hyperons that prefer a spherical shape. At the same time, the Λ hyperon densities get deformed, attracted by the nucleons that prefer a deformed shape. The Si hyper-isotopes are softer against the deformation and its relaxation. The deformation of the Si hyper-isotopes changes more drastically as a function of the Λ hyperon number.

It is also seen that, as Λ hyperons in the p-shell orbitals are more weakly bound than the nucleons, their density spreads out more than that of nucleon in the deformed systems as well as in spherical systems [35–37,39].

There are several directions for future works to explore the generalized nuclear chart with the extra dimensions of hyperons. More systematic investigations on the ground-state structure of multi-Λ nuclei would be interesting. For this purpose, it may be desirable to include Λ-Λ and nucleon-Λ pairing correlations as well as nucleon-nucleon pairing. The possible effects of $NN\Lambda$, $N\Lambda\Lambda$, or $\Lambda\Lambda\Lambda$

three-body forces might also be important for multi-Λ nuclei and neutron-star matter. Other interesting subjects are nuclei with many Σ and/or Ξ hyperons as well as Λ hyperon. An extension of the model and numerical code to such systems is straightforward as long as the interaction is known. To further deepen our knowledge of the general multistrangeness system, collective excitations of multistrangeness nuclei should also be studied with, e.g., GCM (generator coordinate method) or RPA (random-phase approximation) calculations.

ACKNOWLEDGMENT

The author thanks Kouichi Hagino for helpful discussions and comments on the manuscript.

[1] O. Hashimoto and H. Tamura, Spectroscopy of Λ hypernuclei, Prog. Part. Nucl. Phys. **57**, 564 (2006).
[2] A. Gal, E. V. Hungerford, and D. J. Millener, Strangeness in nuclear physics, Rev. Mod. Phys. **88**, 035004 (2016).
[3] G. B. Franklin, Double Λ hypernuclei, Nucl. Phys. A **585**, 83c (1995).
[4] K. Nakazawa for KEK-E176, E373 and J-PARC E07 collaborators, Double-Λ hypernuclei via the Ξ^- hyperon capture at rest reaction in a hybrid emulsion, Nucl. Phys. A **835**, 207 (2010).
[5] M. Danysz, K. Garbowska, J. Pniewski, T. Pniewski, J. Zakrzewski, E. R. Fletcher, J. Lemonne, P. Renard, J. Sacton, W. T. Toner *et al.*, The identification of a double hyperfragment, Nucl. Phys. **49**, 121 (1963).
[6] D. J. Prowse, ${}^{6}_{\Lambda\Lambda}$He Double Hyperfragment, Phys. Rev. Lett. **17**, 782 (1966).
[7] H. Takahashi, J. K. Ahn, H. Akikawa, S. Aoki, K. Arai, S. Y. Bahk, K. M. Baik, B. Bassalleck, J. H. Chung, M. S. Chung *et al.*, Observation of a ${}^{6}_{\Lambda\Lambda}$He Double Hypernucleus, Phys. Rev. Lett. **87**, 212502 (2001).
[8] J. K. Ahn, H. Akikawa, S. Aoki, K. Arai, S. Y. Bahk, K. M. Baik, B. Bassalleck, J. H. Chung, M. S. Chung, D. H. Davis *et al.*, Double-Λ hypernuclei observed in a hybrid emulsion experiment, Phys. Rev. C **88**, 014003 (2013).
[9] H. Ekawa, K. Agari, J. K. Ahn, T. Akaishi, Y. Akazawa, S. Ashikaga, B. Bassalleck, S. Bleser, Y. Endo, Y. Fujikawa *et al.*, Observation of a ${}_{\Lambda\Lambda}$Be double-Λ hypernucleus in the J-PARC E07 experiment, Prog. Theor. Exp. Phys. **2019**, 021D02 (2019).
[10] J. Yoshida, H. Ito, S. Kinbara, H. Kobayashi, D. Nakashima, K. Nakazawa, M. K. Soe, A. M. M. Theint, G. S. Huai, and the J-PARC E07 Collaboration, Exotic nuclei with double strangeness in nuclear emulsion, JPS Conf. Proc. **18**, 011030 (2017).
[11] T. R. Saito, S. Bianchin, O. Borodina, V. Bozkurt, B. Göküzüm, M. Kavatsyuk, E. Kim, S. Minami, D. Nakajima, B. Özel-Tashenov *et al.*, The HypHI phase 0 experiment, Nucl. Phys. A **835**, 110 (2010).
[12] T. Motoba, H. Bandō, and K. Ikeda, Light *p*-shell Λ-hypernuclei by the microscopic three-cluster model, Prog. Theor. Phys. **70**, 189 (1983).
[13] T. Motoba, H. Bandō, K. Ikeda, and T. Yamada, Production, structure, and decay of light *p*-shell Λ-hypernuclei, Prog. Theor. Phys. Suppl. **81**, 42 (1985).
[14] K. Ikeda, H. Bandō, and T. Motoba, Multi-strange hypernuclei, Prog. Theor. Phys. Suppl. **81**, 147 (1985).
[15] E. Hiyama, M. Kamimura, K. Miyazaki, and T. Motoba, γ transitions in $A = 7$ hypernuclei and a possible derivation of hypernuclear size, Phys. Rev. C **59**, 2351 (1999).
[16] E. Hiyama, M. Kamimura, Y. Yamamoto, T. Motoba, and T. A. Rijken, $S = -2$ hypernuclear structure, Prog. Theor. Phys. Suppl. **185**, 152 (2010).
[17] Y. Kanada-En'yo, Excitation energy shift and size difference of low-energy levels in *p*-shell Λ hypernuclei, Phys. Rev. C **97**, 024330 (2018).
[18] M. T. Win and K. Hagino, Deformation of Λ hypernuclei, Phys. Rev. C **78**, 054311 (2008).
[19] H.-J. Schulze, M. T. Win, K. Hagino, and H. Sagawa, Hyperons as a probe of nuclear deformation, Prog. Theor. Phys. **123**, 569 (2010).
[20] M. T. Win, K. Hagino, and T. Koike, Shape of Λ hypernuclei in the (β, γ) deformation plane, Phys. Rev. C **83**, 014301 (2011).
[21] M. Isaka, M. Kimura, A. Dote, and A. Ohnishi, Deformation of hypernuclei studied with antisymmetrized molecular dynamics, Phys. Rev. C **83**, 044323 (2011).
[22] B.-N. Lu, E.-G. Zhao, and S.-G. Zhou, Quadrupole deformation (β, γ) of light Λ hypernuclei in a constrained relativistic mean field model: Shape evolution and shape polarization effect of the Λ hyperon, Phys. Rev. C **84**, 014328 (2011).
[23] M. Isaka, H. Homma, M. Kimura, A. Doté, and A. Ohnishi, Modification of triaxial deformation and change of spectrum in ${}^{25}_{\Lambda}$Mg caused by the Λ hyperon, Phys. Rev. C **85**, 034303 (2012).
[24] M. Isaka, M. Kimura, A. Doté, and A. Ohnishi, Splitting of the *p* orbit in triaxially deformed ${}^{25}_{\Lambda}$Mg, Phys. Rev. C **87**, 021304(R) (2013).
[25] J.-W. Cui, X.-R. Zhou, L.-X. Guo, and H.-J. Schulze, Investigation of single-Λ and double-Λ hypernuclei using a beyond-mean-field approach, Phys. Rev. C **95**, 024323 (2017).
[26] H. Mei, K. Hagino, J. M. Yao, and T. Motoba, Disappearance of nuclear deformation in hypernuclei: A perspective from a beyond-mean-field study, Phys. Rev. C **97**, 064318 (2018).
[27] D. Vretenar, W. Pöschl, G. A. Lalazissis, and P. Ring, Relativistic mean-field description of light Λ hypernuclei with large neutron excess, Phys. Rev. C **57**, R1060(R) (1998).
[28] F. Minato and K. Hagino, Application of random-phase approximation to vibrational excitations of double-Λ hypernuclei, Phys. Rev. C **85**, 024316 (2012).
[29] H. Mei, K. Hagino, J. M. Yao, and T. Motoba, Microscopic particle-rotor model for the low-lying spectrum of Λ hypernuclei, Phys. Rev. C **90**, 064302 (2014).
[30] F. Minato, S. Chiba, and K. Hagino, Fission of heavy Λ hypernuclei with the Skyrme-Hartree-Fock approach, Nucl. Phys. A **831**, 150 (2009).
[31] F. Minato and S. Chiba, Fission barrier of actinide nuclei with double-Λ particles within the Skyrme-Hartree-Fock method, Nucl. Phys. A **856**, 55 (2011).
[32] R. H. Dalitz and A. Gal, Supersymmetric and Strangeness Analog States in *p*-Shell Λ Hypernuclei, Phys. Rev. Lett. **36**, 362 (1976); **36**, 628(E) (1976).
[33] H. Bandō, K. Ikeda, and T. Motoba, Hypernuclear cluster Structure: Di-"Lambpha" system, Prog. Theor. Phys. **66**, 1344

(1981); Microscopic study of Lambpha ($\alpha_\Lambda \equiv {}^{6}_{\Lambda\Lambda}$He) and di-$\alpha_\Lambda$ cluster states, **67**, 508 (1982).
[34] K. Miyahara, K. Ikeda, and H. Bando, Molecular orbital model study of the ${}^{9}_{\Lambda}$Be, ${}^{10}_{\Lambda\Lambda}$Be, ${}^{11}_{3\Lambda}$Be, and ${}^{12}_{4\Lambda}$Be hypernuclei, Prog. Theor. Phys. **69**, 1717 (1983).
[35] M. Rufa, J. Schaffner, J. Maruhn, H. Stöcker, W. Greiner, and P.-G. Reinhard, Multi-Λ hypernuclei and the equation of state of hypermatter, Phys. Rev. C **42**, 2469 (1990); **43**, 2020(E) (1991).
[36] J. Schaffner, C. Greiner, and H. Stöcker, Metastable exotic multihypernuclear objects, Phys. Rev. C **46**, 322 (1992).
[37] J. Mareš and J. Žofka, Multi-strange systems in relativistic mean fields, Z. Phys. A **345**, 47 (1993).
[38] J. Schaffner, C. B. Dover, A. Gal, C. Greiner, D. J. Millener, and H. Stöcker, Multiply strange nuclear systems, Ann. Phys. **235**, 35 (1994).
[39] H.-F. Lü and J. Meng, Hyperon haloes in hypernuclei in the relativistic continuum Hartree-Bogoliubov theory, Chin. Phys. Lett. **19**, 1775 (2002).
[40] I. Filikhin, V. M. Suslov, and B. Vlahovic, Bound state of the $\alpha\Lambda\Lambda\Xi^0$ system, J. Phys. G: Nucl. Part. Phys. **35**, 035103 (2008).
[41] M. Shoeb and Sonika, Stability of the *s*- and *p*-shell α cluster hypernuclei with strangeness $S = -2$ to -4, J. Phys. G: Nucl. Part. Phys. **36**, 045104 (2009).
[42] E. Khan, J. Margueron, F. Gulminelli, and Ad. R. Raduta, Microscopic evaluation of the hypernuclear chart with Λ hyperons, Phys. Rev. C **92**, 044313 (2015).
[43] J. Margueron, E. Khan, and F. Gulminelli, Density functional approach for multistrange hypernuclei: Competition between Λ and $\Xi^{0,-}$ hyperons, Phys. Rev. C **96**, 054317 (2017).
[44] H. Güven, K. Bozkurt, E. Khan, and J. Margueron, ΛΛ pairing in multistrange hypernuclei, Phys. Rev. C **98**, 014318 (2018).
[45] K. Hagino and J. M. Yao, Structure of hypernuclei in relativistic approaches, in *Relativistic Density Functional for Nuclear Structure*, International Review of Nuclear Physics Vol. 10, edited by Jie Meng (World Scientific Publishing, Singapore, 2016), Chap. 7.
[46] J. Boguta and A. R. Bodmer, Relativistic calculation of nuclear matter and the nuclear surface, Nucl. Phys. A **292**, 413 (1977).
[47] J. Cohen and H. J. Weber, Relativistic σ-ω mean-field theory for hyperons from a quark model, Phys. Rev. C **44**, 1181 (1991).
[48] Z.-X. Liu, C.-J. Xia, W.-L. Lu, Y.-X. Li, J. N. Hu, and T.-T. Sun, Relativistic mean-field approach for Λ, Ξ, and Σ hypernuclei, Phys. Rev. C **98**, 024316 (2018).
[49] J. Mareš and B. K. Jennings, Relativistic description of Λ, Ξ, and Σ hypernuclei, Phys. Rev. C **49**, 2472 (1994).
[50] Y. Tanimura and K. Hagino, Description of single-Λ hypernuclei with a relativistic point-coupling model, Phys. Rev. C **85**, 014306 (2012).
[51] W. Long, J. Meng, N. V. Giai, and S.-G. Zhou, New effective interactions in relativistic mean field theory with nonlinear terms and density-dependent meson-nucleon coupling, Phys. Rev. C **69**, 034319 (2004).
[52] S. Marcos, R. J. Lombard, and J. Mareš, Binding energy of double Λ hypernuclei in relativistic mean field theory, Phys. Rev. C **57**, 1178 (1998).
[53] Y. Tanimura, K. Hagino, and H. Z. Liang, 3D mesh calculations for covariant density functional theory, Prog. Theor. Exp. Phys. **2015**, 073D01 (2015).
[54] Z. X. Ren, S. Q. Zhang, and J. Meng, Solving Dirac equations on a 3D lattice with inverse Hamiltonian and spectral methods, Phys. Rev. C **95**, 024313 (2017).
[55] FFTW website [http://www.fftw.org/].
[56] P.-G. Reinhard and R. Y. Cusson, A comparative study of Hartree-Fock iteration techniques, Nucl. Phys. A **378**, 418 (1982).
[57] V. Blum, G. Lauritsch, J. A. Maruhn, and P.-G. Reinhard, Comparison of coordinate-space techniques in nuclear mean-field calculations, J. Comput. Phys. **100**, 364 (1992).
[58] C. Bottcher, M. R. Strayer, A. S. Umar, and P.-G. Reinhard, Damped relaxation techniques to calculate relativistic bound states, Phys. Rev. A **40**, 4182 (1989).
[59] J. A. Maruhn, P.-G. Reinhard, P. D. Stevenson, and A. S. Umar, The TDHF code Sky3D, Comput. Phys. Commun. **185**, 2195 (2014).
[60] J. W. Eastwood and D. R. K. Brownrigg, Remarks on the solution of Poisson's equation for isolated systems, J. Comput. Phys. **32**, 24 (1979).
[61] A. D. Becke, and K. E. Edgecombe, A simple measure of electron localization in atomic and molecular systems, J. Chem. Phys. **92**, 5397 (1990).
[62] P.-G. Reinhard, J. A. Maruhn, A. S. Umar, and V. E. Oberacker, Localization in light nuclei, Phys. Rev. C **83**, 034312 (2011).
[63] C. L. Zhang, B. Schuetrumpf, and W. Nazarewicz, Nucleon localization and fragment formation in nuclear fission, Phys. Rev. C **94**, 064323 (2016).
[64] B. Schuetrumpf and W. Nazarewicz, Cluster formation in precompound nuclei in the time-dependent framework, Phys. Rev. C **96**, 064608 (2017).
[65] J.-P. Ebran, E. Khan, and T. Nikšić, Localization and clustering in atomic nuclei, J. Phys. G: Nucl. Part. Phys. **44**, 103001 (2017).
[66] P. Jerabek, B. Schuetrumpf, P. Schwerdtfeger, and W. Nazarewicz, Electron and Nucleon Localization Functions of Oganesson: Approaching the Thomas-Fermi Limit, Phys. Rev. Lett. **120**, 053001 (2018).
[67] G. A. Lalazissis, J. König, and P. Ring, New parametrization for the Lagrangian density of relativistic mean field theory, Phys. Rev. C **55**, 540 (1997).
[68] M. M. Sharma, M. A. Nagarajan, and P. Ring, Rho-meson coupling in the relativistic mean field theory and description of exotic nuclei, Phys. Lett. B **312**, 377 (1993).
[69] Y. Sugahara and H. Toki, Relativistic mean-field theory for unstable nuclei with non-linear σ and ω terms, Nucl. Phys. A **579**, 557 (1993).